LHC Project Note 102

August 1997
oliver.bruning@cern.ch

Simulations for the Beam-induced Electron Cloud in the LHC liner

Oliver S. Brüning SL/AP

Keywords: electron cloud, LHC liner, heat load

Summary

The paper presents simulation results for the beam-induced electron cloud in the LHC liner.

1 Introduction

The effect of a beam-induced electron cloud in the LHC was first analysed by O. Gröbner [1] and since then has been investigated in more detail by M. Furman and F. Zimmermann [2][3]. The work in [2] pointed out that for the LHC parameters, the beam-induced electron cloud can produce a serious heat load in the LHC liner. Depending on the reflectivity, the photo yield for the production of photo-electrons and the secondary emission yield, this heat load can vary from 0.2 Watt/meter to more then 15 Watt/meter. The current budget of the cryogenic system is based on an electron cloud-induced heat load of 0.2 Watt/meter and can not tolerate a heat load of more then 0.5 Watt/meter. Thus, the design of the beam screen must assure a heat load which is smaller than this amount. Because the heat load depends on the reflectivity, photo and secondary yield of the beam screen, it is mandatory to get accurate estimates for these parameters before any feed-back can be given back to the design of the beam screen.

In June 1997, a crash program was started at CERN to clarify the open questions and to measure the relevant parameters of the vacuum chamber [8]. An important point in this crash program is to study the influence of the strong magnetic field and the low temperatures in the LHC liner. For this purpose, an experimental setup using a standing wave structure as a source for multipacting will provide measurements with and without a magnetic field and at low temperatures. In all cases, the measurements can only be fully analysed by comparing them with simulation data. To this end, a computer program by F. Zimmermann [2] was modified to provide data on the heat load in the vacuum chamber and to look at a variety of bunch shapes and vacuum chamber geometries. In particular, an option for the simulation of a standing wave excitation in a coaxial wave guide was introduced. The simulation results for the coaxial wave guide will be presented in a seperate paper. The following work presents simulation results for the LHC obtained with this modified program and compares the results with the results of M. Furman and the experimental data from measurements at CERN.

E [eV]	N_b	N_p	σ_x [m]	σ_y [m]	σ_z [m]	b_s [ns]	b_l [m]	B [T]	E_γ [eV]
7000	2835	10^{11}	0.303	0.303	0.075	25	14.2	8.4	44.1

Table 1: *Beam parameters for the LHC. E is the beam energy, N_b is the number of bunches in the storage ring, N_p the number of particles per bunch, σ_x, σ_y and σ_z are the horizontal, vertical and longitudinal bunch sizes, b_s is the bunch distance in seconds, b_l the bending magnet length, B the bending field at top energy and E_γ the critical energy of the synchrotron light photons.*

2 Comparison with Analytical Estimates

First estimates of the heat load in the LHC beam screen are based on the following parameters and assumptions: The number of photons emitted by a charged particle per radian is given by [4]

$$N_\gamma = \frac{5}{2\sqrt{3}}\alpha\gamma, \tag{1}$$

where α is the fine-structure constant and γ the Lorenz factor. Thus, for the LHC at 7 TeV the linear photon flux is approximately 10^{17} photons per second and meter. Neglecting secondary emission and reflectivity, the linear heat load is given by

$$< P > = < E_{pe} > \cdot y \cdot 10^{17} eV/s/m, \tag{2}$$

where $< E_{pe} >$ is the average electron energy and y the photo yield. Measurements for a Cu-coated beam pipe at room temperature using synchrotron radiation from the EPA ring (with critical energy close to the LHC value of 44.1 eV) give a photo-yield of $y \approx 0.02$ [8]. Thus, neglecting reflectivity, one gets approximately 2×10^{15} photo-electrons per second per meter. Assuming furthermore a uniform electron cloud in the vacuum chamber, the average energy gain after a bunch passage per electron is approximately 700 eV [5]. Inserting these numbers into Equation (2) we get a linear heat flow of

$$< P > \approx 0.2\ W/m. \tag{3}$$

Table 1 summarises the relevant beam parameters of the LHC.

However, the simulations for the LHC beam show that the assumption of a uniform electron distribution is not justified without secondary emission. As the first bunch passes through the vacuum chamber, low energy ($\sim 5\ eV$) photo-electrons are generated near the surface of the vacuum chamber. In the simulation we assumed a uniform angular distribution of the photo-electrons, as it can be expected for a high reflectivity of the vacuum chamber. Furthermore, we assumed a truncated Gaussian bunch distribution and divided each bunch in 50 slices, each generating a number of photo electrons which is proportional to the total number of protons in the slice. The photo-electrons are accelerated by the field of the following slices. The left-hand side of Fig. 1 shows the resulting energy distribution in the electron cloud without magnetic field for the case of a circular beam pipe and the right-hand side the corresponding velocity distribution. In both cases it was assumed that the photoelectrons are initially at rest and are only accelerated by the following bunch slices. In [5] it was shown that in such a case the velocity distribution should be uniform for a circular beam pipe, independent of the bunch shape. The picture in the right-hand side of Fig. 1 agrees nicely with this expectation.

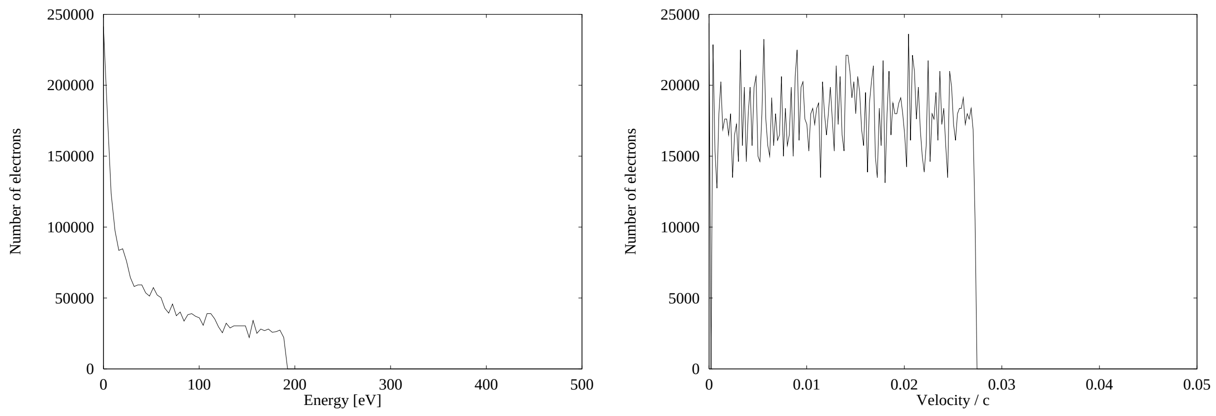

Figure 1: *Circular beam pipe without magnetic field and with photo electrons which are initially at rest. Single bunch passage.*
Left: The energy distribution for the photo-electrons of a Gaussian bunch.
Right: The corresponding uniform velocity distribution.

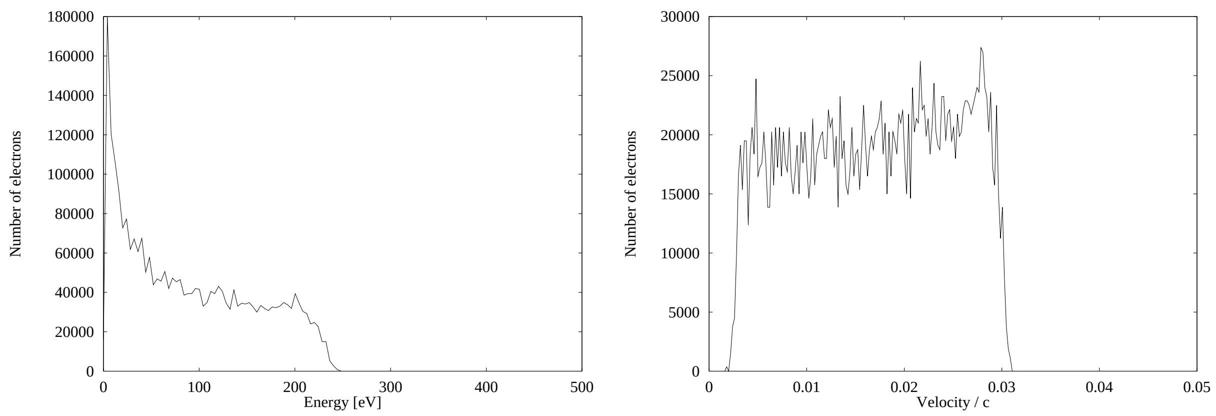

Figure 2: *Circular beam pipe without magnetic field and photo-electrons which have an initial energy distribution. In the simulation we assumed a Gaussian energy distribution around 3 eV with an rms width of 0.5 eV. Single bunch passage.*
Left: The energy distribution for the photo-electrons of a Gaussian bunch.
Right: The corresponding velocity distribution.

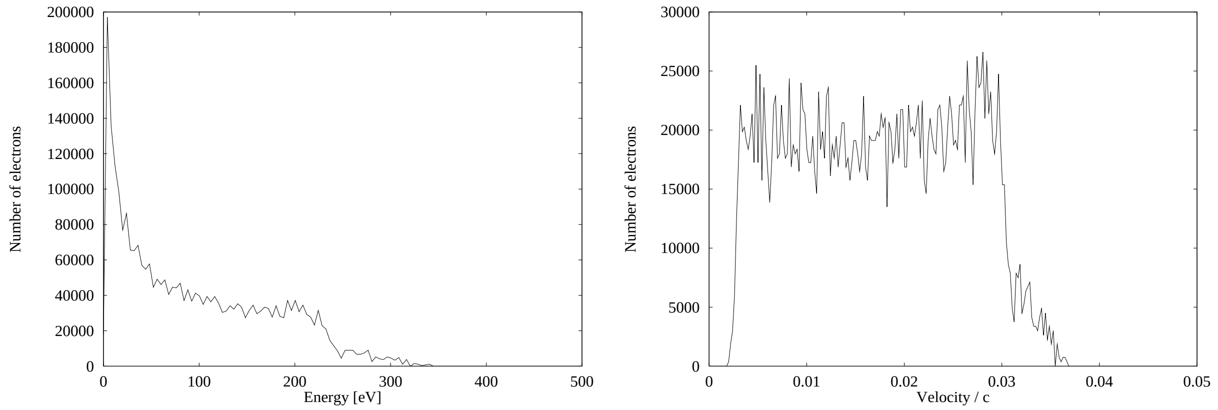

Figure 3: *The LHC-type vacuum chamber without magnetic field. Single bunch passage.*
Left: The energy distribution for the photo-electrons of a Gaussian bunch.
Right: The corresponding velocity distribution.

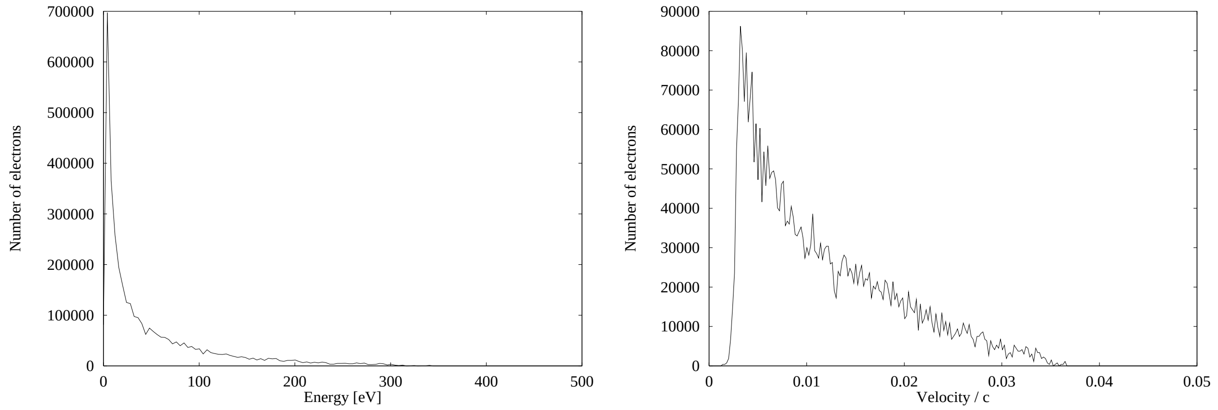

Figure 4: *The LHC-type vacuum chamber with a vertical magnetic field of 8.4 T. Single bunch passage.*
Left: The energy distribution for the photo-electrons of a Gaussian bunch.
Right: The corresponding velocity distribution.

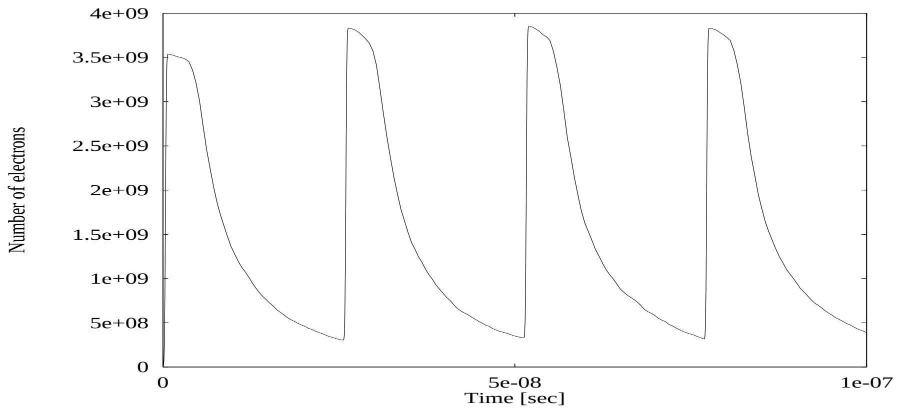

Figure 5: *The number of photo-electrons per bending magnet versus time for the LHC vacuum chamber with magnetic field, a photo emission yield of 0.1 and no secondary emission.*

Fig. 2 shows the same pictures for the case where the photo-electrons already have an initial energy distribution. In the simulation we assumed a Gaussian energy distribution around 3 eV with an rms width of 0.5 eV for the photo-electrons. In this case the velocity distribution shows small deviations from the uniform distribution in Fig. 1. Fig. 3 and Fig. 4 show the corresponding distributions for the LHC beam pipe (including an initial energy distribution of the photo-electrons). Fig. 3 shows the distributions for the case without a magnetic field and Fig. 4 for the case with a vertical magnetic field of 8.4 T. From the left-hand side of Fig. 4 one can see that for the LHC liner most photo-electrons have an energy smaller then 10 eV. The vertical chamber height of the LHC beam screen is 39 mm and the bunch distance in the LHC is 25 ns. Thus, all photo-electrons with a velocity larger then 0.005 c will be absorbed by the vacuum chamber before the next bunch passes by. In other words, without secondary emission, more then 90 % of the photoelectrons are absorbed before the next bunch passes and the remaining electrons have energies smaller then 10 eV. Fig. 5 shows the number of photo-electrons per bending magnet versus time for four bunch passages and without secondary yield. One clearly sees how the number of photo-electrons decreases in between bunch passages and how the maximum number of photo-electrons reaches an equilibrium after only two bunch passages. Looking at Fig. 4, we find that the average electron energy in the electron cloud is less then 50 eV, reducing the estimate for the linear heat load in Equation (2) to

$$< P > \approx 0.015 \; W/m. \tag{4}$$

In the case of a non-negligible reflectivity, the measured photo yield can be too small if the photo-electrons produced at higher reflection levels are not detected [6]. In order to correct for this effect, we follow here the procedure in [2] and define the effective quantum yield by

$$\tilde{Y} = y \cdot \frac{1}{1-R}, \tag{5}$$

where y is the measured photo yield and R the reflectivity. Thus replacing the photo yield in Equation (2) by the effective quantum yield, we get for a reflectivity of $R = 0.8$ (80 % of the photons are reflected)

$$< P > \approx 0.075\ W/m, \tag{6}$$

which is still small compared to the estimate in Equation (3).

However, a realistic heat load can only be estimated if a secondary electron emission is included. In this case, the photo-electrons which hit the vacuum chamber produce new electrons at low energies. These secondary electrons move so slowly that they will still be left when the next bunch passes. In this case, the distribution of the electrons in the vacuum chamber depends on the secondary yield. In the following we will assume that the energy of the secondary electrons is independent from the energy of the incident photo-electrons. Only the yield depends on the energy of the photo electrons and the secondary emission translates the energy distribution of the initial photo-electrons into a density modulation in the electron cloud.

Furthermore, for a small reflectivity, the synchrotron light should preferably hit the outer side of the vacuum chamber and the initial angular distribution of the photo-electrons will not be uniform. This aspect should be remembered when introducing reflectivity in the numerical simulations. In the presence of a strong vertical magnetic field such a situation implies that most photo-electrons are confined to the outer side of the vacuum chamber and that the average energy gain during a bunch passage will be small. In practice, however, it will be difficult to simulate the angular distribution of the photons for different values of the reflectivity. First, we could not yet measure the angular distribution of the photons as a function of the reflectivity and second, the final angular distribution will also depend on the closed orbit in the machine. We will therefore take a conservative approach in the numerical simulations and neglect the effect of the reflectivity on the initial angular distribution of the photo-electrons, resulting in an overestimate of the heat load for a small reflectivity.

3 The Electron Cloud with Secondary Yield

The secondary yield depends on the particle energy and on the incident angle of the photo electron with the surface normal. The analytic expression for the yield is [7]

$$\delta\left(E,\theta\right) = \delta_{max} \cdot 1.11 \cdot \left(\frac{E}{E_{max}}\right)^{-0.35} \cdot \left(1 - exp\left[-2.3 \cdot \left(\frac{E}{E_{max}}\right)^{1.35}\right]\right) / \cos\theta, \tag{7}$$

where θ is the angle of the incident electron with respect to the surface normal, E the electrons energy, E_{max} the energy for which the secondary emission yield has a maximum and δ_{max} the maximum secondary emission yield for normal incidence of the electron. The θ dependence of the secondary yield implies a strong influence of the shape of the vacuum chamber on the electron cloud density.

In order to illustrate this effect of the vacuum chamber geometry on the secondary yield and the electron cloud density, we consider at the LHC-type vacuum chamber and an elliptical chamber. The left-hand side of Fig. 6 shows the LHC-type vacuum chamber and the right-hand side the elliptical vacuum chamber. In the following we assume an effective quantum yield of $\tilde{Y} = 0.02$ and a secondary yield of $\delta_{max} = 1.3$ and $E_{max} = 400\ eV$. Fig. 7 shows the evolution of the number of electrons in the chamber versus time for both cases. The left-hand side shows the case of the LHC-type vacuum chamber and the right-hand side the case of an elliptical vacuum chamber. Both simulations are done with magnetic field and space charge, so that the electron

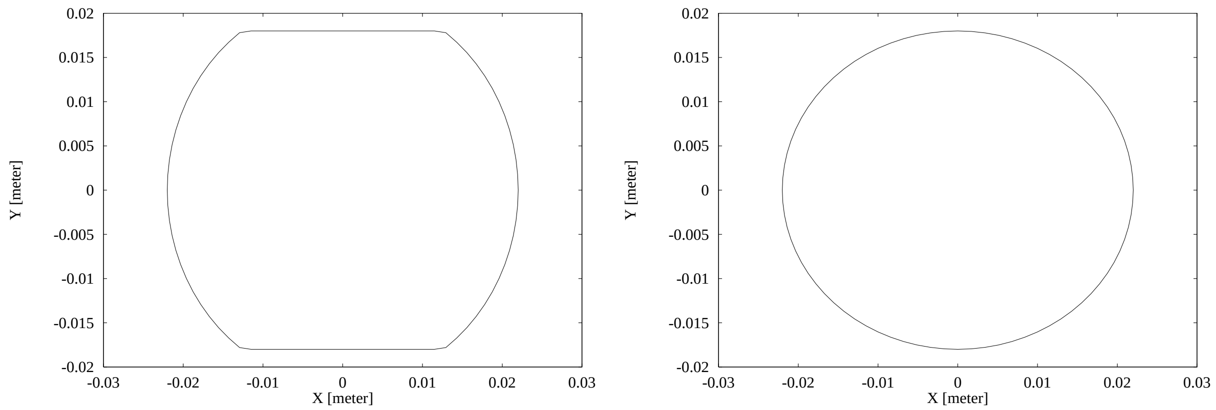

Figure 6: *Left: The geometry of the LHC-type vacuum chamber.*
Right: An elliptical vacuum chamber with comparable dimensions.

cloud distribution reaches a quasi equilibrium, where the number of electrons oscillates up and down between two bunch passages. Due to the different geometries of the vacuum chambers, both cases have clearly different electron densities and result in different heat loads. For the case of the LHC-type vacuum chamber the heat load is approximately 0.2 W/m, while the heat load for the elliptical vacuum chamber is more then 3.0 W/m.

Fig. 8 shows the average secondary yield after 60 bunch passages for the LHC-type vacuum chamber as a function of the horizontal position of the electrons. The left-hand side shows the case of the LHC-type vacuum chamber and the right-hand side the corresponding distribution for an elliptical vacuum chamber with comparable dimensions. While the secondary yield is clearly larger than one for the central region of the elliptical vacuum chamber the secondary yield of the LHC-type vacuum chamber is always smaller then one. The jump in the secondary yield for the LHC-type vacuum chamber is caused by the abrupt change of the surface normal at the transition from flat to curved vacuum chamber. The two maxima of the secondary yield near the center of the beam pipe correspond to the horizontal positions where the average energy gain is close to the energy for which the secondary yield has a maximum. Fig. 9 shows the energy distribution of the electrons that hit the vacuum chamber as a function of their horizontal position. The average electron energy is approximately $< E_{el,LHC} >= 310.0\ eV$ and $< E_{el,Elip} >= 290.0\ eV$ for the LHC-type and an elliptical vacuum chamber respectively. In both cases E_{max} in Equation (7) was set to 400 eV. However, due to the different geometries, the energy distribution for the LHC-type vacuum chamber is narrower then the distribution of the elliptical vacuum chamber. Fig. 10 shows the corresponding horizontal electron distributions for the two cases. In both cases, the horizontal distributions follow the behaviour of the secondary yield in Fig. 8 and are clearly non-uniform. However, the density variation is much more pronounced in the case of the elliptical vacuum chamber.

Both examples illustrate the necessity to incorporate the secondary yield and its dependence on the geometry in estimates for the heat load.

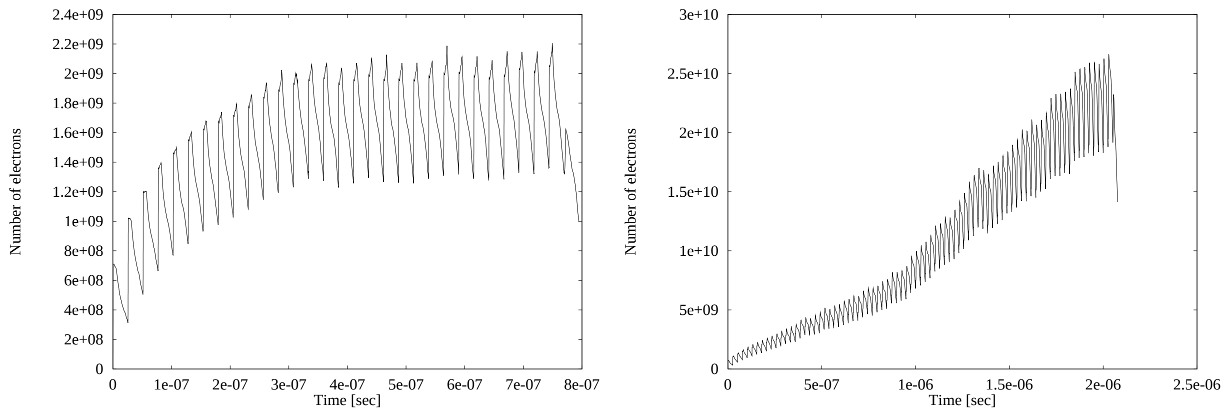

Figure 7: *The number of electrons per bending magnet versus time. Both simulations are done with magnetic field and space charge.*
Left: The LHC-type vacuum chamber.
Right: An elliptical vacuum chamber with comparable dimensions.

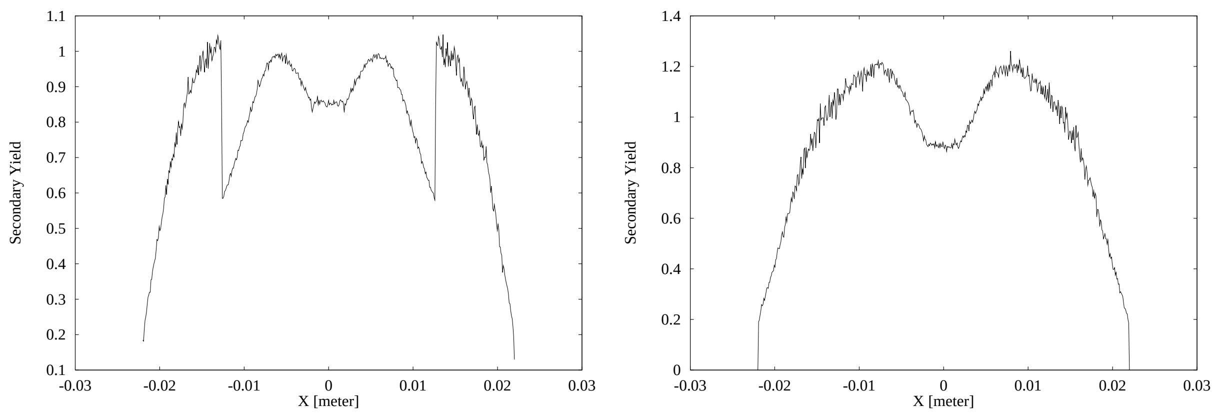

Figure 8: *The average secondary yield after 60 bunch passages as a function of the horizontal electron position.*
Left: The LHC-type vacuum chamber.
Right: An elliptical vacuum chamber with comparable dimensions.

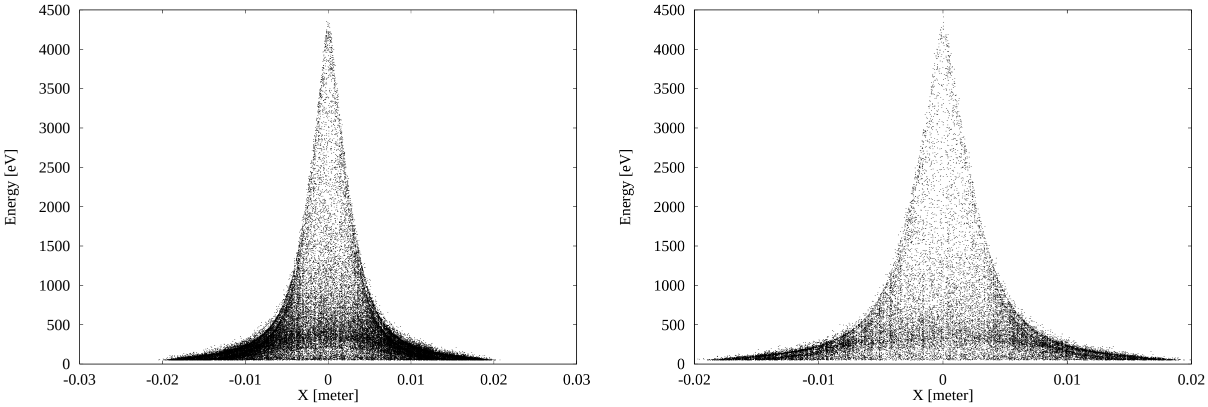

Figure 9: *The energy distribution after 60 bunch passages as a function of the horizontal position. Both simulations are done with magnetic field and space charge.*
Left: The LHC-type vacuum chamber.
Right: An elliptical vacuum chamber with comparable dimensions.

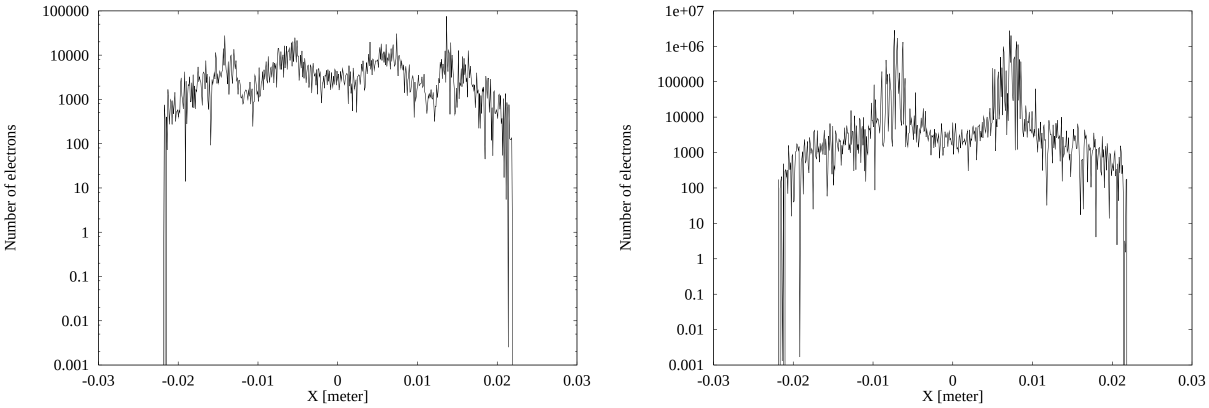

Figure 10: *The horizontal distribution of the electrons after 60 bunch passages on a logarithmic vertical scale.*
Left: The LHC-type vacuum chamber.
Right: An elliptical vacuum chamber with comparable dimensions.

Slices	Steps	bunch passages	$E_{photo,min}[eV]$	$E_{photo,max}[eV]$	$E_{Y,min}[eV]$	$E_{Y,max}[eV]$
50	50	60	0.0	10.0	0.0	20.0

Table 2: *Parameters for the numerical simulations in Fig. 11 to Fig. 13.* $E_{photo,min}$ *and* $E_{photo,max}$ *are the minimum and maximum energies for the photo-electrons respectively and* $E_{Y,min}$ *and* $E_{Y,max}$ *are the minimum and maximum energies for the secondary electrons respectively.*

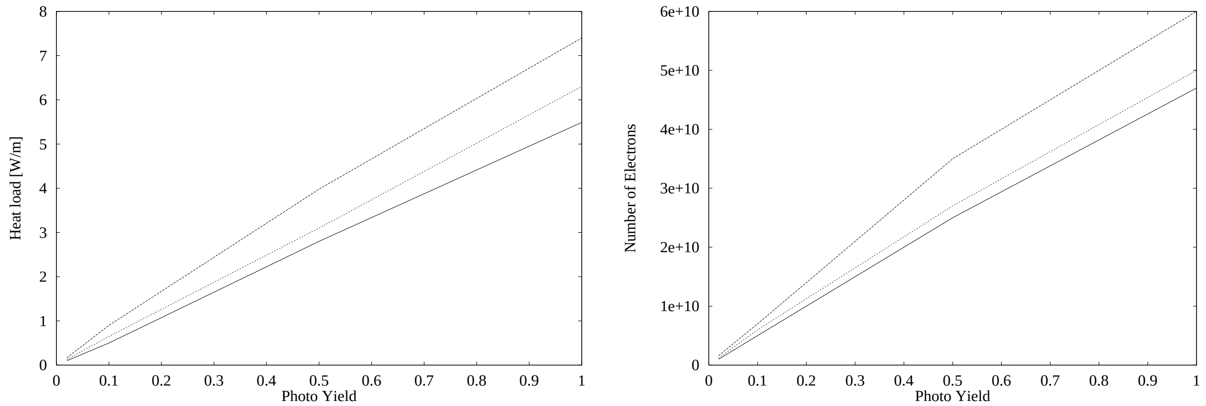

Figure 11: *The heat load and number of electrons versus photo yield for a secondary yield of* $\delta_{max} = 1.066$. *The upper curve describes the case of a circular chamber, the middle curve an elliptical and the lower curve the LHC-type vacuum chamber. Left: The heat load as a function of the effective photo yield. Right: The final number of electrons as a function of the effective photo yield.*

4 Results from Numerical Simulations

Fig. 11 to 13 show the calculated heat loads and number of particles in the electron cloud for different parameters. Fig. 11 shows the heat load versus photo yield $\tilde{Y}$ for the secondary yield of TiN ($\delta_{max} = 1.066$), Fig. 12 for a secondary yield of $\delta_{max} = 1.3$ and Fig. 13 for $\delta_{max} = 1.5$. The upper curve describes the case of a circular chamber with radius $r = 0.022\ m$, the middle curve an elliptical chamber with a horizontal and vertical half axis of $a = 0.022\ m$ and $b = 0.018\ m$ respectively and the lower curve the LHC-type vacuum chamber. In all cases, the photo-electrons had a uniform initial energy distribution between 0 eV and 10 eV and the secondary electrons a uniform initial energy distribution between 0 eV and 20 eV. We used the beam parameters from Table 1 for the nominal LHC beam. Each bunch was cut into 50 slices and the simulation performed 50 intermediate steps in between two bunch passages. Table 2 summarises the relevant parameters. In all cases, the heat load increases proportionaly to the number of electrons in the vacuum chamber and the LHC-type chamber results in a smaller heat load then the elliptical and circular chamber. The effect of the chamber geometry on the heat load is particularly strong for a secondary yield of $\delta \approx 1.3$ and small values of the photo yield $\tilde{Y}$.

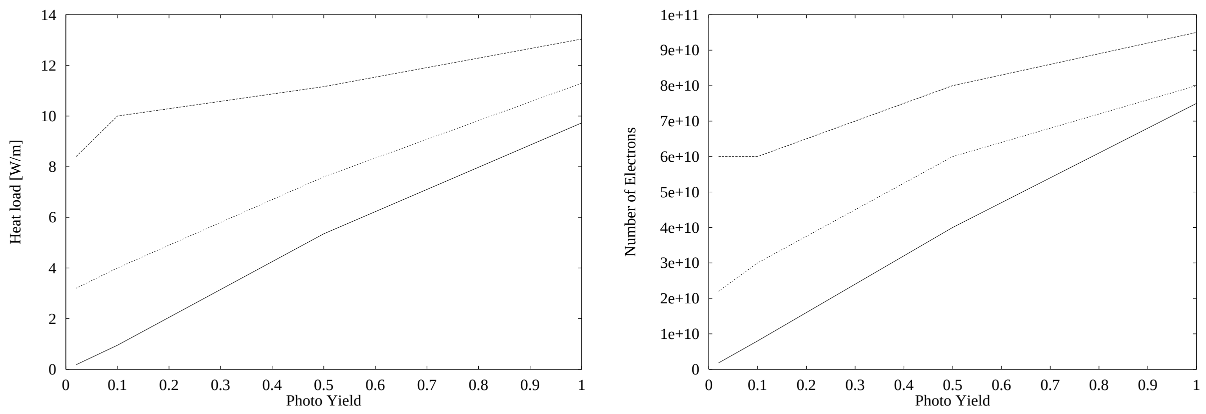

Figure 12: *The heat load and number of electrons versus photo yield for a secondary yield of* $\delta_{max} = 1.3$. *The upper curve describes the case of a circular chamber, the middle curve an elliptical and the lower curve the LHC-type vacuum chamber. Left: The heat load as a function of the effective photo yield. Right: The final number of electrons as a function of the effective photo yield.*

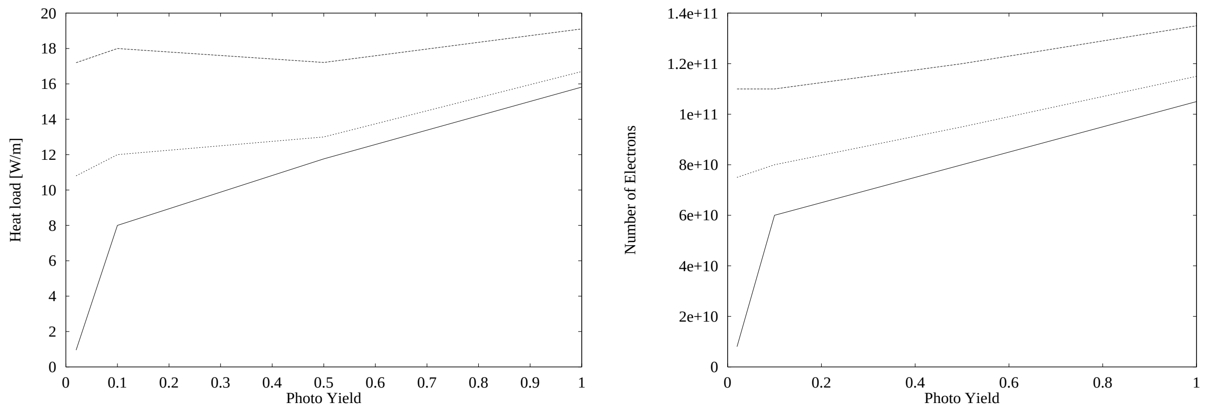

Figure 13: *The heat load and number of electrons versus photo yield for a secondary yield of* $\delta_{max} = 1.5$. *The upper curve describes the case of a circular chamber, the middle curve an elliptical and the lower curve the LHC-type vacuum chamber. Left: The heat load as a function of the effective photo yield. Right: The final number of electrons as a function of the effective photo yield.*

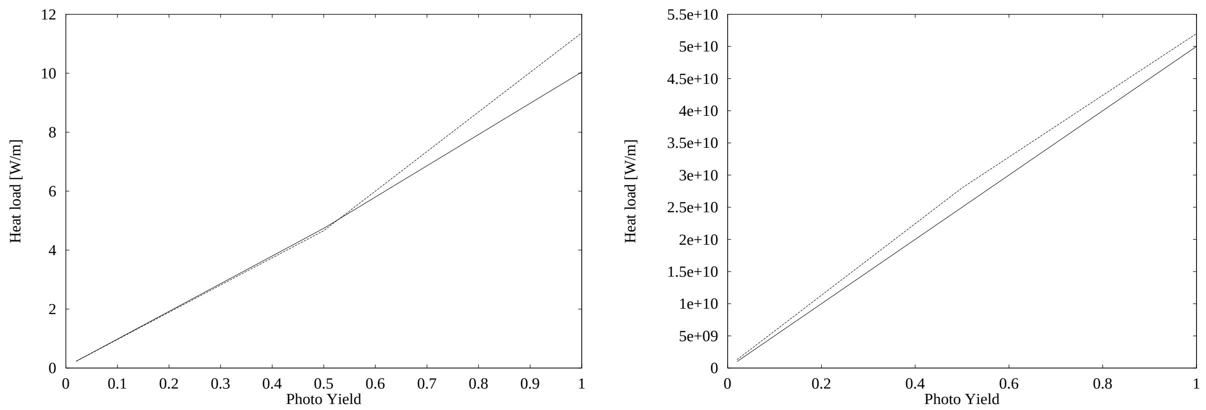

Figure 14: *The heat load and number of electrons versus photo yield for a secondary yield of* $\delta_{max} = 1.066$ *with one slice per bunch. The upper curve describes the case of an elliptical chamber and the lower curve the LHC-type vacuum chamber. Left: The heat load as a function of the effective photo yield. Right: The final number of electrons as a function of the effective photo yield.*

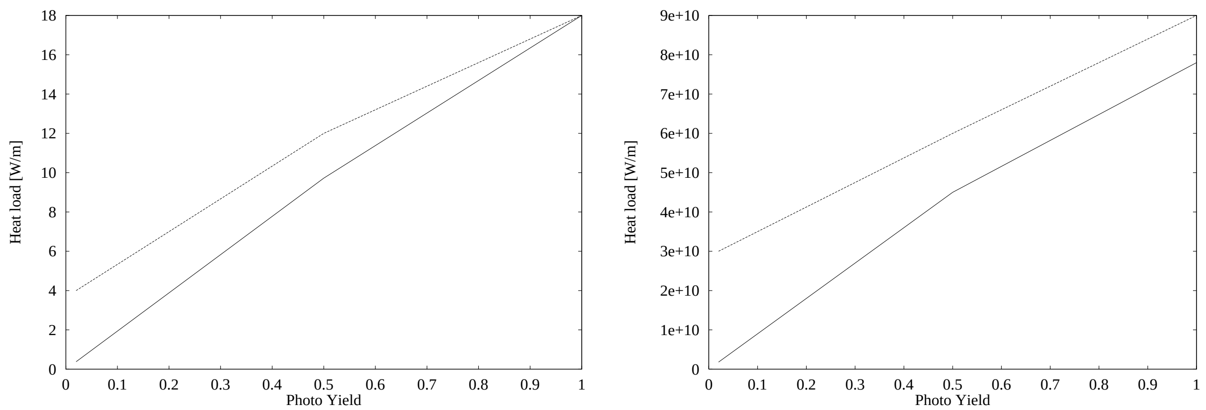

Figure 15: *The heat load and number of electrons versus photo yield for a secondary yield of* $\delta_{max} = 1.3$ *with one slice per bunch. The upper curve describes the case of an elliptical chamber and the lower curve the LHC-type vacuum chamber. Left: The heat load as a function of the photo yield. Right: The final number of electrons as a function of the photo yield.*

Comparing the results for an elliptical vacuum chamber from Fig. 11 and 12 with the results in [2] one finds that the results in Fig. 11 and 12 are approximately a factor 2 smaller than the results in [2]. It might be that this difference is related to the different number of slices in the simulation. If we reduce the number of slices to one slice per bunch, we obtain heat loads which are roughly a factor 2 larger. Fig. 14 and 15 show the corresponding results for a secondary yield of TiN ($\delta_{max} = 1.066$) (Fig. 14) and $\delta_{max} = 1.3$ (Fig. 15). in both cases, the lower curve corresponds to the LHC-type and the upper curve to an elliptical vacuum chamber.

Another potential source for this difference is the initial energy distribution of the photo-electrons and secondary electrons. If we change, for example, the initial energy distribution of the photo-electrons from a uniform to a Gaussian distribution with an rms width of 0.5 eV centered around 2.0 eV, we can also get a heat load which is a factor two larger than the results in Fig. 11 to 13.

5 Discussion

A TiN coating is a viable option for the LHC beam screen [8]. Thus, assuming a secondary yield of $\delta_{max} = 1.066$, keeping the heat load lower then 0.5 W/m requires an effective photo yield of $\tilde{Y} < 0.1$. However, recent measurements at CERN have shown that the effective photo yield is more likely to be $\tilde{Y} \approx 0.2$, which would increase the heat load for the nominal beam to almost 1 W/m. For the ultimate LHC beam with $1.6 \cdot 10^{11}$ protons per bunch the situation is even worse, where an effective photo yield of $\tilde{Y} = 0.1$ and a secondary yield of $\delta_{max} = 1.066$ results in a heat load of 3.5 W/m.

Comparing the results for different vacuum chamber geometries showed that for the case of a small photo yield the final heat load can vary by more then one order of magnitude. In these cases, the LHC-type vacuum chamber always gave the smallest heat load. However, other geometries could be analysed in order to minimize the heat load.

Furthermore, the simulations showed that the initial energy distributions for the photo- and secondary electrons can change the final heat load by a factor of two. The discussion in [3] showed that for the critical energy of the LHC photons a wide energy distribution (almost uniformly distributed between 0 eV and 20 eV) is a good approximation for the photo electrons. In this case the heat load is only half the value obtained for a narrow energy distribution around 2 eV.

First measurements at CERN indicate that the strong vertical magnetic field will reduce the photo and secondary emission yield if the magnetic field lines run parallel to the surface. However, for the LHC-type vacuum chamber this mainly affects the surfaces left and right from the beam, where the energy gain due to the electron-beam interaction is small (see Fig. 9). Therefore, the electrons in these regions are not critical for the heat load to begin with. In order to reduce the heat load one either has to reduce the photo and secondary emission yield at the flat part of the LHC beam screen (above and below the beam) where the energy gain due to the electron-beam interaction is large, or one has to avoid a creation of electrons in this region in the first place. Thus, one potential cure for the electron-induced heat load is to constrain the photons of the synchrotron light to a small layer around the mid-horizontal plane of the vacuum chamber. In this case all photo-electrons are generated at the left and right side of the vacuum chamber and can not enter the central part of the chamber. However, at his point it is not clear how this could be achieved.

One interesting result from the simulations was that an additional DC electric field in the vertical direction can significantly reduce the heat load. For example, assuming an effective photo yield of $\tilde{Y} = 0.1$ and a secondary yield of $\delta_{max} = 1.5$, an additional DC electric field in the vertical direction with 20 V between the upper and lower boundary of the vacuum chamber can reduce the heat load of the LHC-type vacuum chamber from 8 W/m to less then 0.5 W/m. After the photo-electrons hit the vacuum chamber only low eneregy electrons are present. In this case, even a small electric field in the vertical direction can significantly modify the electron distribution in the vacuum chamber. On the one side of the vacuum chamber the electrons are pulled back to the vacuum chamber. On the other side, the electrons are accelerated and they can reach the other side of the vacuum chamber before the next bunch passes by.

A last resort would be to reduce the maximum number of protons per bunch and thus the maximum energy gain of the electrons during the electron-beam interaction. Assuming an effective photo yield of $\tilde{Y} = 0.1$ and a secondary yield of $\delta_{max} = 1.5$ one has to reduce the bunch intensity to $0.6 \cdot 10^{11}$ protons per bunch in order to limit the heat load to 0.2 W/m. Assuming an effective photo yield of $\tilde{Y} = 0.2$ and a secondary yield of $\delta_{max} = 1.066$, one also has to reduce the bunch intensity to $0.6 \cdot 10$ 11 protons per bunch. Because the maximum luminosity depends on the square of the number of particles per bunch, such a solution would lead to a considerable reduction of the maximum luminosity and exclude the operation with the 'ultimate' bunch current of $1.6 \cdot 10^{11}$ particles per bunch. The loss in luminosity could partially be recovered by a smaller transverse emittance. However, because the luminosity increases only linearly with decreasing emittance, one still has a linear reduction of the luminosity with the bunch current [9].

References

[1] O. Gröbner 'Technological problems related to the cold vacuum system of the LHC', Vacuum, vol. 47, pp. 591-595 (1996)

[2] M. Furman 'The Electron-Cloud Effect for LHC' Proceedings of the international workshop on multibunch instabilities in future electron and positron accelerators, Tsukuba, Japan 1997.

[3] F. Zimmermann 'A Simulation Study of Electron-Cloud instability and Beam-Induced Multipactoring in the LHC' LHC Project Report 95

[4] M. Sands, 'The physics of Electron Storage Rings', SLAC-121 (1970)

[5] J.S. Berg 'Energy Gain in an Electron Cloud During the Passage of a Bunch' LHC Project Report 97

[6] J.B. Jeanneret, 'Photoemission in LHC - A simple model', CERN SL/Note 97-48 (AP)

[7] H. Seiler, 'Secondary electron emission in the scanning electron microscope', Phys. 54 (11) (1983)

[8] F. Ruggiero http://wwwslap.cern.ch/collective/electron-cloud/electron-cloud.html

[9] Yellow book, CERN/AC/95-05 (LHC)